RSC Advances

ROYAL SOCIETY OF CHEMISTRY

www.rsc.org/advances

Preparation of keratin/chlorhexidine complex nanoparticles for long-term

and dual stimuli-responsive release

Xuelian Zhi, Yanfang Wang, Pengfei Li, Jiang Yuan*, Jian Shen*

Jiangsu Key Laboratory of Biofunctional Materials, College of Chemistry and Materials Science, Nanjing Normal University, Nanjing 210023, China

*Corresponding authors: bioalchem@yahoo.com(Yuan), jshen@njnu.edu.cn(Shen)

Tel. +86 25 85891536; Fax. +86 25 83599188

1 Introduction

Keratin is a chief component found in hair, skin, fur, wool, horn, and feathers. It has a high content of cysteine, serine, and a large number of hydroxyl amino acids. Keratin based biomaterials have emerged as potential candidates for many biomedical and biotechnological applications due to their intrinsic biocompatibility, biodegradability, mechanical durability, and natural abundance[1]. Keratin based films can be used as a wound dressing[2,3], implantable devices coating [4,5], cell encapsulant[6,7], and ocular surface reconstruction[8,9]. Keratin-based hydrogels are neuroinductive and capable of facilitating regeneration in a peripheral nerve injury model in mice[10,11]. Keratin hydrogels can also act as a hemostatic agent in a rabbit model of lethal liver injury[12], a carrier for rhBMP-2[13], and a platform for antibiotic[14]. Keratin-based fibers have the potential usage for tissue engineering scaffold. Due to its poor mechanical property, keratin is usually composited with biodegradable polymers such as poly (3-hydroxybutyrate-co-3-hydroxyvalerate)[15], poly(lactic acid)[16], and poly (ε-caprolactone)[17].

Keratin should be an ideal drug carrier due to its advantages such as good biocompatibility, biodegradability, absorbability, and non-immunogenicity. In addition, keratin is rich negative charged, which is favor for electrostatic absorping the positive small molecules, such as acid salt typed drugs. Furthermore, the large amount of carboxyl groups within the keratin endows it as a pH responsive smart drug carrier candidate. However, little work has been done on keratin-based drug carrier. Van Dyke group have described the delivery and activity of the antibiotic ciprofloxacin delivered from keratin hydrogel[14]. Wang group have prepared keratin hydrogel and film for controlling drug release[18,19]. Liu group have synthesized poly(ethylene glycol)(PEG) and poly(*N*-(2-hydroxypropyl)methacrylamide)(PHPMA) grafted keratin used for dual reduction and enzyme responsive drug carriers[20, 21].

Various methods have been used to prepare protein-based nanoparticles such as desolvation[22], nanoprecipitation[23], self-assembly[24], and so on. Among them, desolvation and nanoprecipitation procedure need to use organic solvents or additives, which may cause the protein denatured. For self-assembly procedure, protein and drug solutions are directly mixed to allow their interaction based on specific forces such as hydrogen bonding and hydrophobic interactions. For our modified keratin, a large amount of carboxy groups (-COO$^-$) of which can strongly attract the cationic drug. This electrostatic complexation leads to the formation of nanoparticles. Based on electrostatic interaction, Malek et al. [25] have prepared cisplatin-incorporated nanoparticles with drug-induced ionic gelation technique. Ionic gelation

technique has been used widely to prepared chitosan nanoparticles[26-32]. To the best of our knowledge, it has not yet been reported to prepare protein nanoparticles with this method.

Chlorhexidine(CHX) is widely used to treat and prevent skin and mucosal infections with a low toxicity. In dentistry, it has been recognized as a gold standard against antiplaque and gingivitis for three decades[33]. Due to its cationic charge, CHX is used as a drug model. The purpose of this study is to develop a facile method to fabricate stable keratin-based drug delivery systems without any chemical cross-linkers and surfactants. Herein, keratin/CHX complex nanoparticles(KCNPs) were prepared by drug induced ionic gelation technique via electrostatic interactions(Fig.1). Then, the size, zeta potential, and drug-loading capacity of KCNPs were characterized with DLS, SEM, and TEM. MTT assay was used to evaluate their cell toxicity. The pH dependent CHX delivery behavior was tested at pH 5.29, 7.4 and 9.18, respectively. The glutathione(GSH) sensitive release behavior was also tested at pH 7.4. These KCNPs are potential for long-term and controlled release of CHX for antibacterial applications.

Figure 1

2. Materials and methods

2.1 Materials

Chlorhexidine acetate ($C_{22}H_{30}N_{10}Cl_2 \cdot 2C_2H_4O_2$) was supported by Aladdin (Shanghai, China) with a purity of 98%. *E. coli* (ATCC 25922) and *S. aureus* (ATCC 25923) were provided by Jiangsu Provincial Center for Disease Prevention and Control, China. All other chemicals were of analytical grade and were used without further purification.

2.2 Extraction of keratin[2, 34, 35]

Human hair was washed with soap and 70% ethanol to remove surface oil, followed by rinsed extensively with water and dried and then cut into short pieces. The pretreated hair was mixed with urea, sodium dodecyl sulfate (SDS), 2-mercaptoethanol and water. The mixture was kept stirred for 48 h at 65 °C and then filtered. Subsequently, the filtrate was dialysed against deionized water for 48 h to afford a colorless solution. The dialysate was then allowed to react with iodoacetic acid for stability. Finally, this dialysate was dialysed again and lyophilized to obtain S-(carboxymethyl) keratin. The molecular weight of keratin was analyzed by SDS–polyacrylamide gel electrophoresis (PAGE).

2.2 Preparation of KCNPs

KCNPs were prepared by ionic gelation process. Keratin and CHX were dissolved in an aqueous solution to obtain a stock solution with a final concentration of 1 mg/mL, respectively. Then, CHX solution was added dropwise at a speed of 1.5 mL/h under constant stirring to keratin solution according to ratio listed in Table 1, followed by stirring for 60 min and storage at room temperature overnight. The mixture was dialyzed for 1 day to remove unstable adsorbed CHX. Subsequently, free CHX dialysate were measured by ultraviolet spectrometer for CHX loading content and encapsulation efficiency. The dialysate was lyophilized for future studies. The drug loading content(LC) and drug encapsulation efficiency(EE) were calculated according to the following equations:

$$LC\,(\%) = \frac{Total\quad drug - Free\quad drug}{Nanoparticles\quad weight} \times 100\%$$

$$EE\,(\%) = \frac{Total\quad drug - Free\quad drug}{Total\quad drug} \times 100\%$$

2.3 Characterization of KCNPs

The infrared spectra of keratin and KCNPs were recorded within the range of 4000-400 cm^{-1} by a Perkin-Elmer FT-IR spectrometer in KBr. Hydrodynamic diameter distribution and Zeta potentials of nanoparticles were determined by dynamic light scattering (DLS) method using a Malvern Zetasizer Nano ZS90 system (Malvern Instruments Company Limited，British), in which freeze-dried KCNPs were dispersed in different pH of phosphate buffer solution. All analyses were triplicated and the results were the average of the three runs. The morphology of KCNPs was observed by transmission electron microscopy (TEM, JEM-100S, JEOL, Japan) and scan electron microscopy (SEM, Hitachi SU 3500, Japan).

2.4. In vitro pH independent CHX release study

100 mg of KCNPs in 5 mL buffer solution was placed into dialysis bag (MWCO 3500). Subsequently, dialysis bag was dipped into receptor compartment containing 200 mL dissolution medium, which was shaken gently at 37±0.5 ℃. Then, the medium was adjusted to pH 5.29 PBS, pH 7.4 PBS, and pH 9.18 sodium tetraborate buffer to test the release of CHX, respectively. The receptor compartment was closed to prevent the evaporation losses from the dissolution medium. Periodically, 3 mL of release medium was withdrawn and 3 mL of fresh PBS was added to the system. The CHX concentration in the sampled medium was determined by UV spectrometer with absorption at a wavelength of 260 nm.

2.5 In vitro GSH sensitive CHX release study

Regarding the GSH senstive delivery, similar procedure is followed as above except the presence of GSH. The concentrations of GSH both inside and outside the dialysis bag were kept at 10 uM and pH 7.4 PBS solution during the release experiments to mimic the redox conditions in blood plasma. At certain time intervals, CHX concentrations of the outer side of the dialysis bag were determined by UV spectrometer with absorption at wavelength of 260 nm.

2.6 Bacterial inhibition

The antimicrobial activity of KCNPs was investigated against *E. coli* as the model Gram-negative bacteria and *S. aureus* as the model Gram-positive bacteria by disc diffusion method. The bacteria were incubated in nutrient agar at 37 ℃ to reach 10^6 CFU/mL. Agar plates were streaked with a sterile swab moistened with KCNPs. Then the bacteria were coated on the agar surface evenly and the plates were incubated overnight at 37 ℃. The reaction of the microorganisms to the KCNPs was determined by the size of the inhibitory zone. When the materials have an excellent antibacterial activity, the inhibitory zones are very large.

2.7 Cytotoxicity assay by MTT

The cytotoxicity of KCNPs against NIH-3T3 cell was evaluated using MTT assay. The cells in a DMEM medium containing 10% fetal bovine serum (FBS, Gibco) and 1% penicillin G -streptomycin were seeded into 96-well flat-bottomed plates with a density of 1×10^4 cells/well and then were incubated in CO_2 atmosphere at 37 ℃ for 12 h. Next, the medium in each well was removed and samples (100 μl) with various concentrations in DMEM were added to the wells. Subsequently, the cells were incubated for 48 h under the same condition. The medium was replaced with 90 μl of fresh medium with 10 μl of MTT solution (5 mg/mL). After incubation for 4 h, the solution was removed, leaving the precipitate. Then 100 μl of dimethyl sulfoxide (DMSO) was added to each well and oscillated for 30 min in the dark at room temperature. The cell viability was measured by a microplate reader (BioTek Synergy2) at a wavelength of 570 nm.

2.8 Statistical analysis

Results are displayed as means ± standard deviation (SD). Statistical analysis was performed using one-way analysis of variance (ANOVA) with a Tukey posthoc method, and a significant level of $p < 0.05$ was chosen for all the tests.

3. Results and discussion

3.1 Preparation of KCNPs

Generally, keratin can be extracted by an oxidative method or an reduction method. Herein, we extracted

keratin from human hair using the reduction strategy. The molecular weight of extracted keratin was determined by SDS–PAGE analysis(Fig.2). The patterns revealed two major, diffuse clusters of bands: 25 and 40 kDa. So, the molecular weight of keratin was concentrated on ca. 25 and 40 kDa.

Figure 2

The ionic gelation method was used to prepare KCNPs with the different ratios between keratin and CHX as 9/1, 7/3, and 5/5. The stability of resulting KCNPs after 4 h and 14 days standing is shown in Figure S1. It shows that KCNPs at the ratio of 9 and 1 are stable even standing longer as 14 days. As for ratios of 7/3 and 5/5, the prepared nanoparticles are unstable after 14-day standing. So, the ratio to 9 and 1 is fixed for samples preparation.

The drug encapsulation efficiency (EE) and loading content (LC) of KCNPs are listed in Table 1. Generally, a high drug concentration leads to a great drug loading content while a high keratin concentration tends to a decreased drug encapsulation efficiency. Herein, the drug loading content was gradually increased while the encapsulation efficiency was reduced with the increasing mixed ratio between CHX and keratin. For keratin/CHX nanoparticles complexed at the ratio of 9 and 1, EE and LC are 91.2% and 9.2%, respectively. From above results, we can confirm that the cationic drugs can be effectively entrapped in keratin molecules due to their strong electrostatic interaction.

Table 1

3.2 Characterization of KCNPs

3.2.1 FT-IR and UV-Vis **spectra analysis**

The results of FTIR spectra of keratin and KCNPs are shown in Figure S2. Regarding keratin, the characteristic absorption peaks near 1646, 1548 and 1245 cm^{-1} are known as amide I, amide II, and amide III, respectively. Amide I, mainly related to C=O stretching is useful for the analysis of the secondary structure of the proteins. The peaks at 990 cm^{-1} and 614 cm^{-1} are the characteristic absorptions of the C–S and S–S bonds[36, 37]. In the case of KCNPs, there is no shift for amide I peak, indicating the maintainance of keratin conformation.

UV-Vis absorption measurement is a very simple method to explore the structural change and to know the complex formation. In the present study, we have recorded the UV-Vis absorption spectra of keratin and keratin-CHX complexes. In Figure 3, the spectra showed largely blue changed with $\lambda_{max\ fro}$ from 276 nm to

263 nm, which can be related to complex formation between CHX and keratin through hydrogen bonds and electrostatic interaction[38,39].

Figure 3

3.2.2 Size and morphology

The hydrodynamic diameters of the resulting KCNPs in the medium with various pH values are investigated and presented in Table 2. It can be seen that the mean diameter of nanoparticles increases from 163 to 195 nm when the pH value of the medium is changed from 5.29 to 9.18. It may attribute to that the keratin moiety of KCNPs becomes more hydrated and swell caused by deprotonation with the increasing pH value.

Table 2

Typical TEM image of the KCNPs is shown in Figure 4a, from which it can be seen that the KCNPs are solid spheres with the diameter of about 176 nm, which is very close to the result of DLS. Generally, protein molecules exist as a form of colloid in water. As a result, there is no obvious difference between the sizes of the nanoparticles in aqueous medium and in the dry state. The morphology of the KCNPs is also observed by SEM and the results are shown in Figure 4b. A statistics on the particle size gives an average diameter of 170 nm.

Figure 4

3.2.3 Zeta potential measurements

Surface charges and thereby the stabilities of the prepared KCNPs are determined by zeta potential measurements. The zeta-potential directly relates to the net charges on the surface of KCNPs. The zeta potential value for the KCNPs is found to be −39.1 mV. This value lies in the stable range, indicating that the KCNPs are stable and possess negative surface charge. The negative charge is contributed by the excess of carboxyl groups of keratin. The zeta potentials of the KCNPs at different pH values are given in Table 2. The zeta potentials of the KCNPs are −15.3 mV and −29.5 mV in pH range from 5.29 to 9.18 due to the deprotonated carboxyl groups of the keratin. As the pH reaches to 5.29, the net charges on the KCNPs surface are too low to stabilize the nanoparticles, resulting in forming precipitation(Fig. S3).

3.3 In vitro pH independent CHX delivery profile

Keratin seems to be a very appropriate to load CHX due to its rich carboxylic acid groups. Thanks to the electrostatic attraction between the cationic CHX molecules and the anionic keratins,   CHX is accordingly loaded into the KCNPs with a satisfactory drug loading content of 9.2% and an encapsulation efficiency of 91.2%(Table 1). Fig.S4 shows the standard curve of DOX with a high goodness of fit as the function of concentration at 260 nm. To investigate release characteristics of CHX from KCNPs, dialysis method is used. To demonstrate the pH-sensitive release, the release of CHX is studied over a period of 240 h in acidic (PBS, pH 5.29), 120 h in neutral (PBS, pH 7.4), and 120 h in basic (sodium tetraborate buffer, pH 9.18) conditions. Figure 5 shows the whole release profiles of CHX from KCNPs. There are no initial burst release occur, indicating the strong complexation of CHX with keratin.

In PBS with pH value of 7.4, which corresponds to the physiological conditions of the blood stream, only ~23% of CHX is delivery in the initial 100 h (Fig. 5a). The dialysate keeps clear during the whole release period. It indicates that the KCNPs are stable for a long term at physiological pH(Fig. S3). The release of CHX is extraordinary slow in PBS with pH value of 9.18(Fig. 5a). For example, only ~8% of the loaded CHX is released within 100 h, suggesting that CHX release from the KCNPs in basic environment is significantly suppressed. It is because that enhanced negative charges of KCNPs adsorb the CHX tightly, which inhibiting the CHX release.

The release of CHX is even slower at acidic pH 5.29 than at pH 7.4 in the initial 60 h (Fig. 5b). Depending on the protonation of keratin that the carboxylate groups(COO^-) of KCNPs can be converted into the neutral carboxylic acid groups(COOH) by reducing the pH value, the hydrophilicity of KCNPs decrease. So, KCNPs become smaller and denser at pH 5.29 (Table 2), which suppresses the delivery. Thus, the release rate is faster than that at pH 9.18. It is due to the protonation of CHX increases its hydrophilicity, which enhances the delivery. After releasing for the first 60 h, the release rate is speeded sharply. It is due to the synergetic effects of dual protonations of CHX and keratin. The protonation of CHX increases the hydrophilicity of CHX. Meanwhile, the protonation of keratin weakens the electrostatic attraction of CHX. These two above synergetic effects both accelerate the delivery of CHX, resulting in the sharp release. It is interested that the release profile shows a straight line, indicating a constant speed release of CHX. The pharmacokinetic release behavior follows the zero order equation. Fig.S3 shows the effect of pH value on the stability of KCNPs. The KCNPs tend to aggregate and deposit at acidic pH value, which is close to the iso-electric point of keratin. Such pH-sensitive drug release behavior is desirable for tumor treatment since

the ideal antitumor drug release should be slow in the neutral environment of systemic circulation in vivo and relatively faster in the weak acidic environment of tumor tissue[40]. In our study, about 39.5% of CHX is released within 240 h at pH 5.29 condition. These results suggest that keratin-based nanocarriers are satisfactory for a long term anticancer drug loading and release. The possible process of drug release could be expected. The pH-sensitive antitumor drug-loaded KCNPs would be accumulated and released at the tumor site due to the enhanced permeability and retention (EPR) effect.

Figure 5

The release process of CHX may be described with pseudo-first-order kinetic or pseudo-second-order kinetic equations[41]. Pseudo-first-order kinetic equation can be represented in the linear form as

$$\ln(q_e-q_t)=\ln q_e-k_1 t \qquad (1)$$

Where q_e and q_t are the equilibrium release amount and the release amount at any time (t), respectively, and k_1 is the rate constant of pseudo-first-order release kinetics. If the pseudo-first-order kinetics is applicable, the plot of $\ln(q_e-q_t)$ vs. t will be linear, and the k_1 value can be obtained from the slope of the linear plot.

Pseudo-second-order kinetic equation can be represented in the linear form as

$$t/q_t = 1/(k_2 q_e^2) + t/q_e, \qquad (2)$$

Where k_2 is the rate constant of pseudo-second-order release kinetics. If this kinetic is applicable, the plot of t/q_t vs. t will be linear, which allows computation of k_2. Figure 5c shows the plot of t/q_t vs. t for CHX release at pH 7.4 and 9.18. Fair straight lines are obtained and the correlation coefficient of the fitting curve reaches at least 0.991. It is found that the pseudo-second-order model is more satisfactory for describing the release process for simulation of the above two kinetic models for the release kinetic data.

3.4 *In vitro* GSH sensitive CHX release study

The release of CHX was also investigated at GSH concentrations of 10 μM corresponding to the level of GSH in blood plasma and pH 7.4(Fig.6a). It can be seen that about 45% of the loaded CHX can be finally released after reaching the plateau of 100 h. In comparison, only 23% of CHX can be release without GSH at the plateau of 70 h. These results could be attributed to the fact that the disulfide bonds of KCNPs were partially cleaved by GSH through reduction reaction, which resulted in an enhanced release of CHX. Fig. 6b shows the size of KCNPs in the presence of 10 uM GSH at the delivery time of 0 h, 48 h, 72 h, and 120 h. The sizes of KCNPs become larger with the increasing delivery time, indicating the broken disulfide bonds of

KCNPs. The swollen KCNPs lead to a sufficient release of CHX as compared to that at pH 7.4 without GSH. Fig. 6c shows the the accumulated release of CHX at pH 5.29 with and without 10 uM GSH as a function of time. The delivery is accelrated under the action of GSH as compared to that without GSH.

Figure 6

3.5 In vitro cytotoxicity by MTT assay

An antibacterial material requires low toxicity to normal cells at appropriate concentrations for killing bacteria efficiently. Cytotoxicity of KCNPs to fibroblast cells is evaluated using MTT method. As shown in Figure 7, at the lower concentration (2.5 ug/mL of KCNPs, i.e., 0.2 ug/mL of CHX), cell viability of KCNPs is 66% as compared to FBS control, indicating their slight cytotoxicity. However, as the concentration is even higher, it shows significant cytotoxicity. Ostad et al have used endometrial cell to access the cytotoxicity of CHX and CHX-releasing devices. The results indicate that CHX is toxic at the concentration of 1 ug/mL[42]. It is also reported that 0.6 and 20 mg/mL of CHX decrease cell metabolism and viability by 60 and 70 %, respectively[43]. According to our drug loading content data(9.2%), 2.5 ug/mL of KCNPs is the equivalent of 0.23 ug/mL of CHX. It seems that the cytotoxicity of CHX is enhanced when CHX is complexed with keratin.

Figure 7

3.6 Antibacterial test

CHX is used worldwide as a cationic antimicrobial agent against oral microbiota. The antibacterial activity of KCNPs against *E. coli* and *S. aureus* is determined using zone of inhibition method. The disks produced a zone of inhibition clearly (Fig.8). The zone of inhibition for *S. aureus* looks larger than that for *E. coli*. It seems KCNPs have better antibacterial activity against *S. aureus* than *E. coli*. The above results are consistent with the known conclusion that CHX is more effective against Gram-positive microbes than Gram-negative microbes [44].

Figure 8

4. Conclusion

In summary, keratin/CHX complex nanoparticles(KCNPs) are successfully prepared with ca. 180 nm. The CHX release behavior shows these nanoparticles are both pH and GSH sensitive. Under acid and blood

10

plasma level GSH conditions, the KCNPs exhibit more rapid and long term drug release. Moreover, the low concentration of KCNPs show slight cytotoxicity and simultaneously maintain their antibacterial property. In a word, keratin-based drug delivery system can be regarded as a valuable pH-responsive strategy for the delivery of anticancer agents such as doxorubicin hydrochloride salt(DOX・HCl).

Acknowledgements

Reference

[1] J. G. Rouse and M. E. Van Dyke, *Materials*, 2010, **3**, 999-1014.

[2] J. Yuan, J. Geng, Z. Xing, K. J. Shim, I. Han, J. C. Kim, I. K. Kang and J. Shen, *J. Tissue Eng. Regen. Med.*, 2012, doi: 10.1002/term.1653.

[3] A. Vasconcelos, A.P. Pêgo, L. Henriques, M. Lamghari and A. Cavaco-Paulo，*Biomacromolecules*, 2010，**11**, 2213–2220

[4] V. Dyke, Mark E., Siller-Jackson and Arlene, *J. Polymer. Mater. Sci. Eng.*, 2002, **87**, 453-454.

[5] K. Yamauchi, M. Maniwa and T. Mori, *J. Biomater. Sci. Polymer Edn.*, 1998, **3**, 259-270.

[6] K. Yamauchi and A. Khoda, *Colloids Surf. B*, 1997, **9**, 117-119.

[7] R. Silva, B. Fabry and A. R. Boccaccini. *Biomaterials*, 2014, **35**, 6727-6738.

[8] M. Borrelli, N. Joepen, S. Reichl, D. Finis, M. Schoppe, G. Geerling and S. Schrader, *Biomaterials*, 2015, **42**, 112–120.

[9] S. Reichl, M. Borrelli and G. Geerling, *Biomaterials*, 2011, **32**, 3375–3386.

[10] L. A. Koman, A. Atala, M. V. Dyke, P. Sierpinski, J. Garrett, J. Ma, P. Apel, D. Klorig and T. Smith, *Biomaterials*, 2008, **29**,118-128.

[11] P. J. Apel, J. P. Garrett, P. Sierpinski, J. Ma, A. Atala, T. L. Smith, L. A. Koman and M. E. Van Dyke, *J. Hand. Surg.*, 2008, **33**, 1541-1547.

[12] T. Aboushwareb, D. Eberli, C. Ward, C. Broda, J. Holcomb, A. Atala and M. Van-Dyke,   *J. Biomed. Mater. Res.B*, 2009, 90B, 45-54.

[13] C. J. Kowalczewski, S. Tombyln, D. C. Wasnick, M. R. Hughes. M. D. Ellenburg, M. F. Callahan, T. L. Smith, M. E. Van Dyke, L. R. Burnett and J. M. Saul. *Biomaterials,* 2014, **35**, 3220-3228.

[14] J. M. Saul, M. D. Ellenburg, R. C. de Guzman and M. V. Dyke, *J. Biomed. Mater. Res. A*, 2011, **98A**, 544-553.

[15] J. Yuan, Z. C. Xing, S. W. Park, J. Geng, J. Shen, W. Meng, K. J. Shim, I. S. Han, J. C. Kim and I. K. Kang, *Macromol. Res.*, 2009, **17**, 850-855.

[16] J. Yuan, J. Shen and I. K. Kang. *Polym. Int.*, 2008, **57**, 1188-119.

[17] A. Edwards, D. Jarvis, T. Hopkins, S. Pixley and N. Bhattarai, *J. Biomed. Mater. Res. B*, 2015, **103**, 21-30.

[18] J. H. Guo, S. J. Pan, X. C. Yin, Y. F. He, T. Li, R. M. Wang, *J. Appl. Polym. Sci.* 10.1002/app.41572

[19] X. C. Yin, F. Y. Li, Y. F. He, Y. Wang and R. M. Wang, *Biomater. Sci.*, 2013, **1**, 528-536.

[20] Q. M. Li, L. J. Zhu, R. G. Liu, D. Huang, X. Jin, N. Che, Z. Li, X. Z. Qu, H. L. Kang and Y. Huang, *J. Mater. Chem.*, 2012, **22**, 19964–19973.

[21] Q. M. Li, S. N. Yang, L. J. Zhu, H. L. Kang, X. Z. Qu, R. G. Liu and Y. Huang, *Polym. Chem.*, 2015, 6, 2869–2878.

[22] M. Rahimnejad, N. Mokhtarian and M. Ghasemi, *Afr. J. Biotechnol.*, 2009, **8**, 4738–4743.

[23] S. A. Khan and M. Schneider. *Macromol. Biosci.*, 2013, **13**, 455–463.

[24] S. Han, M. Li, X. Liu, H. Gao and Y. Wu, *Colloids Surf. B: Biointerfaces,* 2013, 102, 833–841.

[25] S. J. Malek, R. Khoshchehreh, N. Goodarzi, M. R. Khoshayand, M. Amini, F. Atyabi, M. Esfandyari-manesh, S. Tehrani, R. M. Jafari, M. S. Maghazei, F. Alvandifara, M. Ebrahimi and R. Dinarvand, *Colloids and Surfaces B: Biointerfaces*, 2014, **122**, 350-358.

[26] Andréia Lange de Pinho Neves, C. C. Milioli, L. Müller, H. G. Riella, N. C. Kuhnen, H. K. Stulzer,

Colloids and Surfaces A, 2014, **445**, 34–39.

[27] J. Zhang, C. Tang and C. H. Yin, *Biomaterials*, 2013, **34**, 3667–3677.

[28] E. N. Koukaras, S. A. Papadimitriou, D. N. Bikiaris and G. E. Froudakis, *Mol. Pharmaceutics*, 2012, **9**, 2856–2862.

[29] Y. Hou, J. Hu, H. Park and M. Lee, *J. Biomed. Mater. Res. A*, 2012, **100**, 939–947.

[28] Yaping Hou, Junli Hu, Hyejin Park and Min Lee.

[30] W. Fan, W. Yan, Z. Xu and H. Ni. *Colloids Surf. B: Biointerfaces*, 2012, **90**, 21–27.

[31]F. M. Goycoolea, G. Lollo, C. Remuñán-López, F. Quaglia and M. J. Alonso, *Biomacromolecules*, 2009, **10**, 1736–1743.

[32] Q. Gan, T. Wang, C. Cochrane and P. McCarron, *Colloids Surf. B: Biointerfaces*, 2005, **44**, 65–73.

[33] C. G. Jones, *Periodontol 2000*, 1997, **15**, 55–62.

[34] K. Yamauchi, A. Yamauchi, T. Kusunoki, A. Kohda and Y. Konishi, *J. Biomed. Mater. Res.*, 1996, **31**, 439-444.

[35] P. M. M. Schrooyen, P. J. Dijkstra, R. C. Oberthür, A. Bantjes and J. Feijen, *J. Agric. Food Chem.*, 2000, **48**, 4326-4334.

[36] J. Z. Shao, J. H. Zheng, J. Q. Liu and C. M. Carr, *J. Appl. Polym. Sci.*, 2005, **96**, 1999-2004.

[37] S. W. Ha, A. E. Tonelli and S. M. Hudson, *Biomacromolecules*, 2005, **6**, 1722-1731.

[38] K. Abdi, Sh. Nafisi, F. Manouchehri, M. Bonsaii and A. Khalaj, *J. Photochem. Photobiol. B*, 2012, **107**, 20–26.

[39] S. Bakkialakshmi and D. Chandrakala, *Spectrochimica Acta Part A*, 2012, **88**, 2–9.

[40] C. J. T. Hoes, J. Grootoonk, R. Duncan, I. C. Hume, M. Bhakoo, J. M. W. Bouma and J. Feijen, *J. Controlled Release*, 1993, **23**, 37-53.

[41] L. Dong, L. Yan. W. G. Hou and S. J. Liu, *J. Solid State Chem.*, 2010, **183**, 1811–1816.

[42] S. N. Ostad and P. R. Gard, *J. Pharm. Pharmacol.*, 2000, **52**, 779–784.

[43] F. C. R. Lessa, A. M. F. Aranha, I. Nogueira, E. M. Giro, J. Hebling and C. A. Costa, *J. Appl. Oral Sci.*, 2010, **18**, 50–58.

[44] G. J. Christensen, *J. Am. Dent. Assoc.*, 2002, **133**, 229-231.

Table Caption

Table 1 Parameters of as-prepared KCNPs

Table 2 Size and zeta potential of KCNPs by DLS

Table 1 Parameters of as-prepared KCNPs

Samples	EE (%)	LC (%)
Weight ratio of keratin and CHX=9:1	91.2	9.2
Weight ratio of keratin and CHX=7:3	64.1	21.5
Weight ratio of keratin and CHX=5:5	46.1	31.6

Table 2 Size and zeta potential of KCNPs by DLS
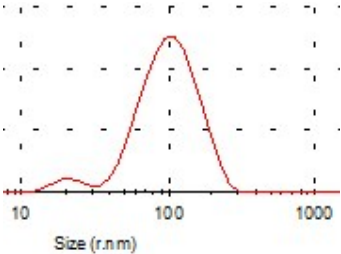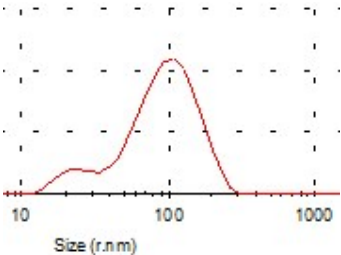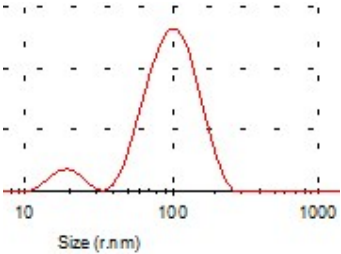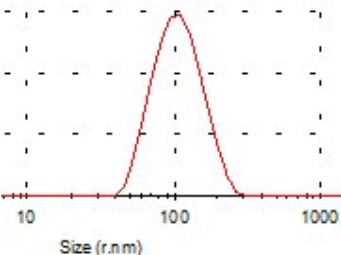
pH value	Size Distribution by intensity	PDI	Z-Average (d. nm)	Zeta potential (mV)
7.0		0.260	180	-39.1±1.5
5.29		0.394	163	-15.3±1.5
7.4		0.365	185	-15.5±0.6
9.18		0.299	195	-29.5±1.4

Figure Caption

Fig.1 Schematic representation of preparation of keratin/CHX complex nanoparticles(KCNPs) by ionic gelation method.

Fig. 2 The electrophoresis separation patterns of the human hair keratin by SDS-PAGE assay.
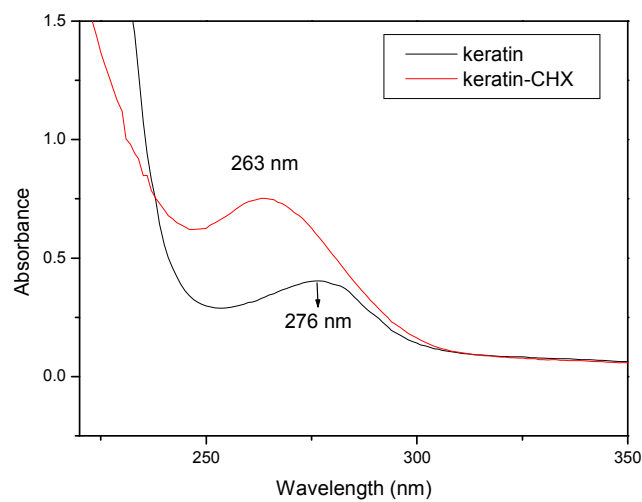
Fig.3 UV-Vis spectra of keratin and KCNPs.

Fig.4 TEM(a) and SEM(b) images of KCNPs.

Fig.5 Release profile of CHX from KCNPs. (a) Release profile at pH 7.4 and 9.18; (b) Release profile at pH 5.29; (c) Linear regression curves of release data fitting with pseudo-second kinetic mode for KCNPs.

Fig. 6 (a) Release profile at pH 7.4 with and without 10 uM GSH; (b) Size of KCNPs by DLS at pH 7.4 and 10 uM GSH with the delivery time of 0 h, 48 h, 72 h, and 120 h; (c) Release profile at pH 5.29 with and without 10 uM GSH.

Fig.7 Cell viability of KCNPs at various concentration to NIH-3T3 cells growth determined by MTT viability assay (* indicates significant difference at $p < 0.05$ level).

Fig. 8 Antibacterial inhibition zone of KCNPs against *E. coli* (a) and *S. aureus* (b)

Fig.1 Schematic representation of preparation of keratin/CHX complex nanoparticles(KCNPs) by ionic gelation method.
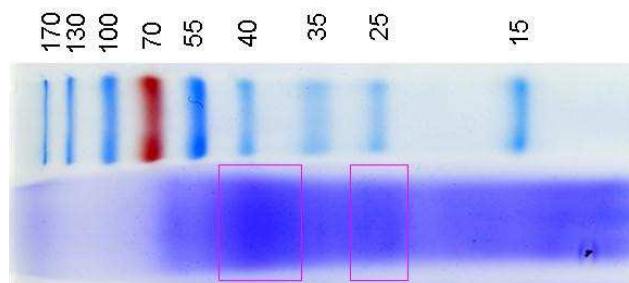
Fig. 2 The electrophoresis separation patterns of the human hair keratin by SDS-PAGE assay.
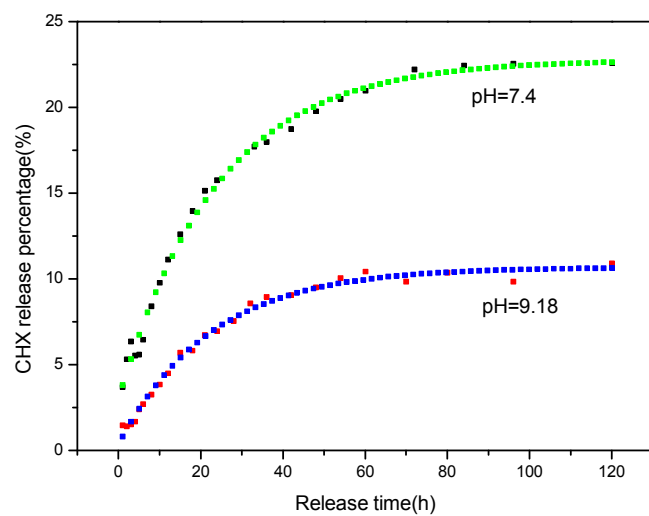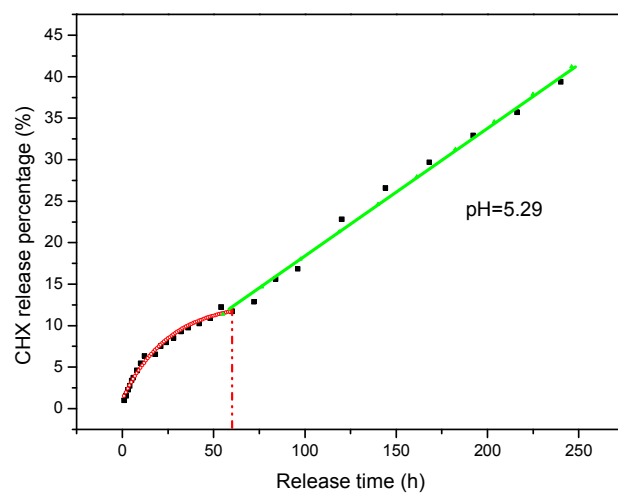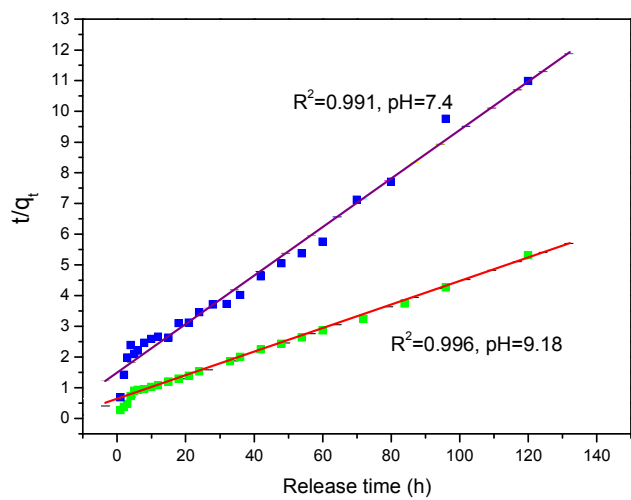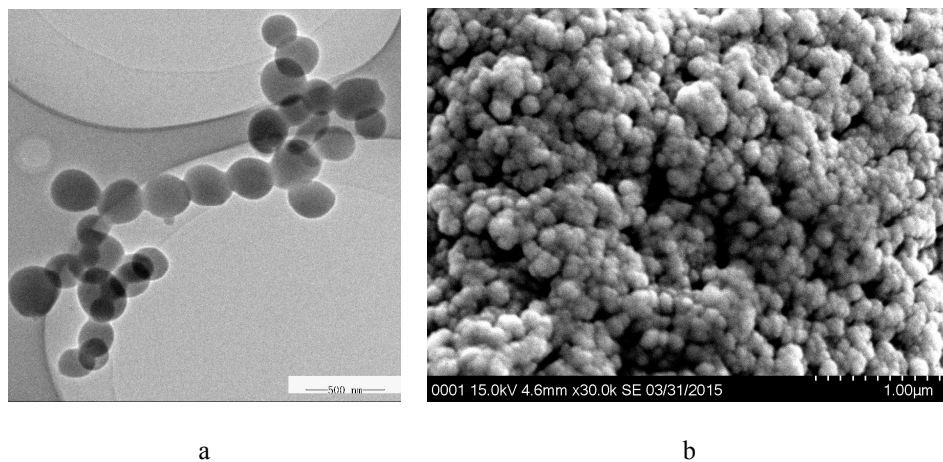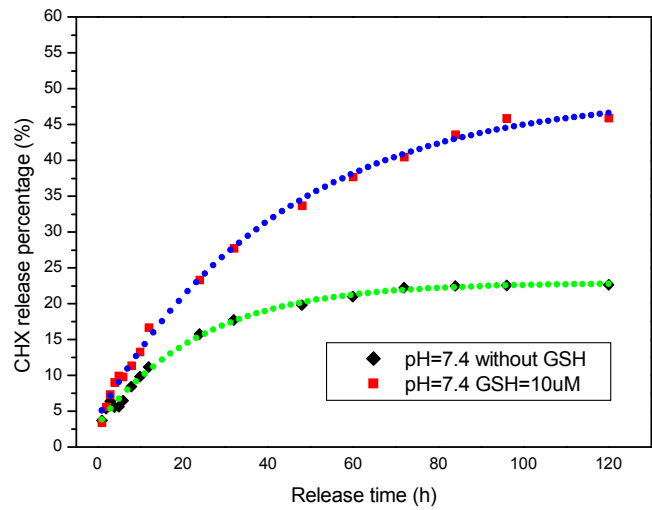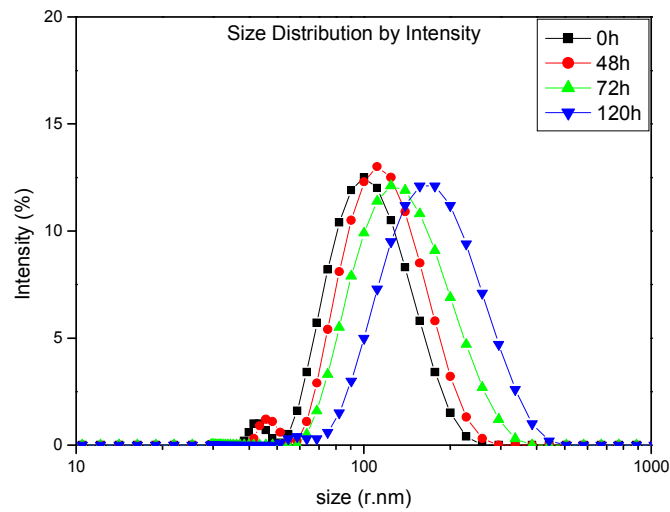
Fig.3 UV-Vis spectra of keratin and KCNPs.

a

b

c

Fig.5 Release profile of CHX from KCNPs. (a) Release profile at pH 7.4 and 9.18; (b) Release profile at pH 5.29; (c) Linear regression curves of release data fitting with pseudo-second kinetic mode for KCNPs.
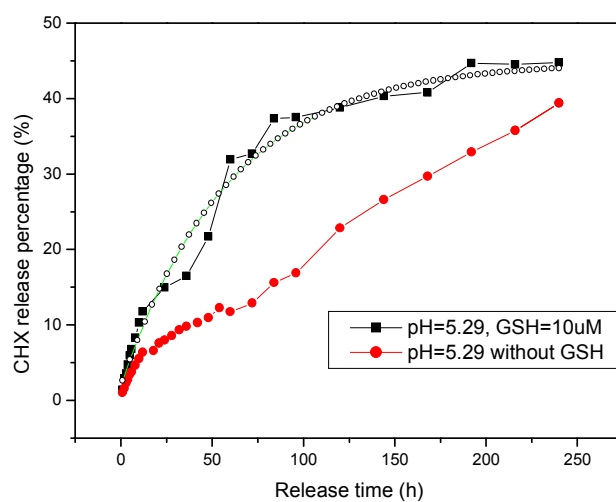
a   b

Fig.4 TEM(a) and SEM(b) images of KCNPs.

a

b

c

Fig. 6 (a) Release profile at pH 7.4 with and without 10 uM GSH; (b) Size of KCNPs by DLS at pH 7.4 and 10 uM GSH with the delivery time of 0 h, 48 h, 72 h, and 120 h; (c) Release profile at pH 5.29 with and without 10 uM GSH.
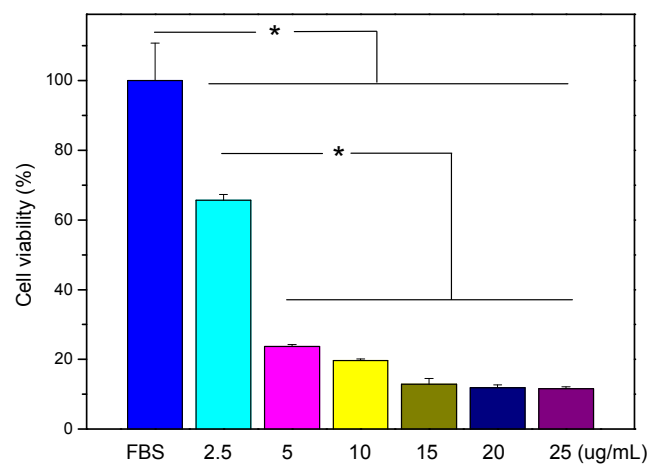
Fig.7 Cell viability of KCNPs at various concentration to NIH-3T3 cells growth determined by MTT viability assay (* indicates significant difference at $p < 0.05$ level).
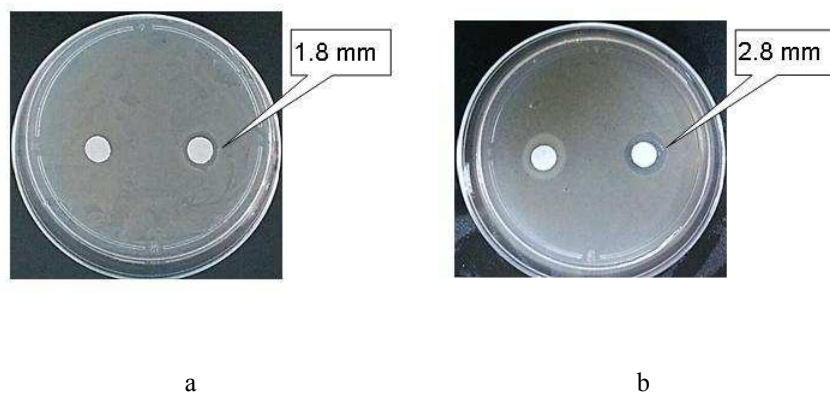
Fig. 8 Antibacterial inhibition zone of KCNPs against *E. coli* (a) and *S. aureus* (b).